Supporting Information

Effective calcium doping at B-site of $BaFeO_{3-\delta}$ perovskite: Towards low-cost and high-performance oxygen permeation membrane

Yao Lu[a], Hailei Zhao*[ab], Kui Li[a], Xuefei Du[a], Yanhui Ma[a], Xiwang Chang[c], Ning Chen[a], Kun Zheng[d], and Konrad Świerczek[d]

[a]School of Materials Science and Engineering, University of Science and Technology Beijing, Beijing 100083, China. *E-mail: hlzhao@ustb.edu.cn; Fax: +86 10 82376837; Tel: +86 10 82376837

[b]Beijing Municipal Key Laboratory of New Energy Materials and Technologies, Beijing 100083, China

[c]State Key Laboratory of Advanced Metallurgy, University of Science and Technology Beijing, Beijing 100083, China

[d]Department of Hydrogen Energy, Faculty of Energy and Fuels, AGH University of Science and Technology, al. A. Mickiewicza 30, 30-059 Krakow, Poland

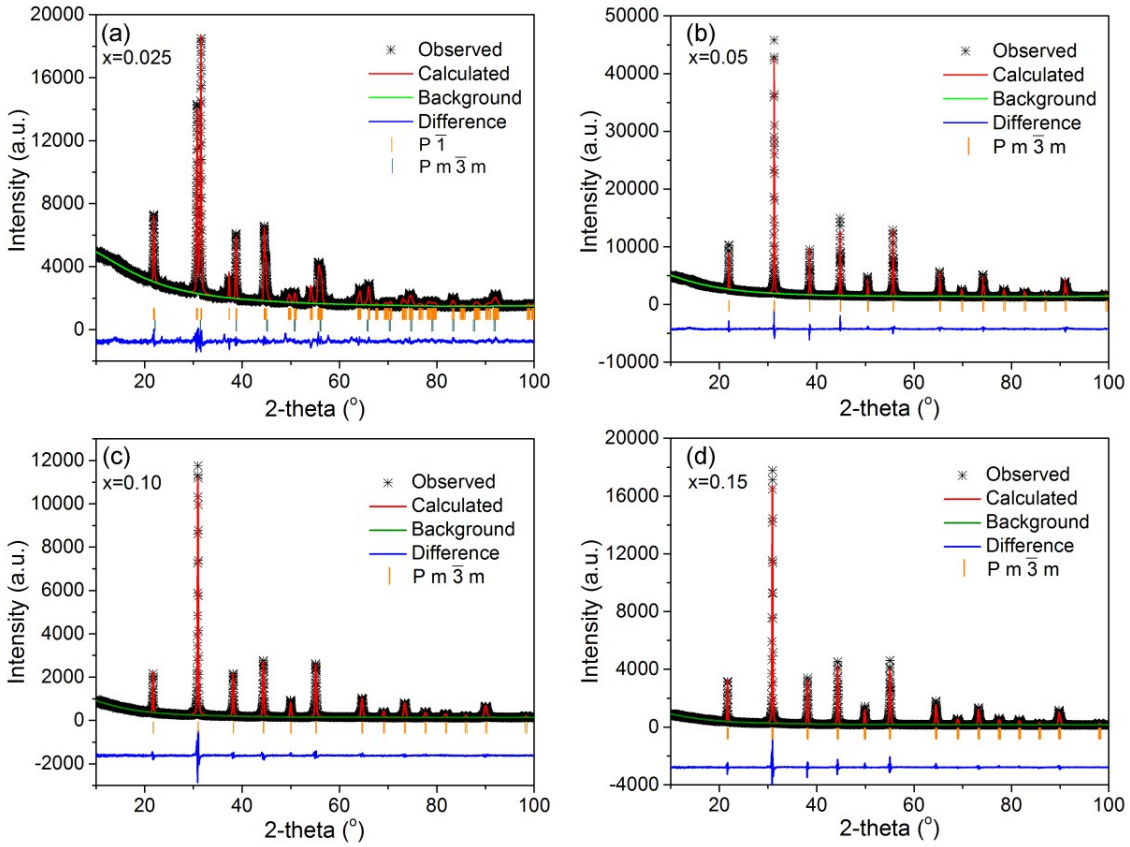

Fig. S1 Refined XRD profiles of (a) x=0.025, (b) x=0.05, (c) x=0.10, (d) x=0.15 samples at 25 ˚C.

The structure of x = 0.025 can be approximated by mixed dual phase of triclinic distorted perovskite and distortionless cubic perovskite, but presence of superstructure-related peaks is obvious. One of the possible super-structural approximations is P2 $2\sqrt{2}\times2\sqrt{2}\times1$ supercell, however, reliable refinement of all atomic coordinates was not possible. For samples x = 0.05-0.15, a high goodness of fit with cubic perovskite structure was obtained.

Table S1 Detailed refinement results of x = 0.025-0.15 sample at 25 ˚C

	Element	Site	x	y	z	Uiso (Å^2)
x=0.025 χ^2=3.328 R_p=2.77 % wR_p=3.85 %	$P\bar{1}$(76.3 *wt*%), a=4.0654(3) Å, b=4.0599(3) Å, c=4.0344(2) Å, α=88.49(1) º, β=88.50(1) º, γ=88.30(1) º					
	Ba	1a	0	0	0	0.0258(12)
	Fe	1h	0.5	0.5	0.5	0.0577(22)
	Ca	1h	0.5	0.5	0.5	0.0577(22)
	O1	1e	0.5	0.5	0	0.0237(2)
	O2	1f	0.5	0	0.5	0.0500(5)
	O3	1g	0	0.5	0.5	0.0289(4)
	$Pm\bar{3}m$(23.7 *wt*%), a=b=c=4.0138(3) Å, α=β=γ=90 º					
	Ba	1a	0	0	0	0.0138(6)
	Fe	1b	0.5	0.5	0.5	0.0187(10)
	Ca	1b	0.5	0.5	0.5	0.0187(10)
	O	3c	0.5	0.5	0	0.0599(22)
x=0.05 χ^2=2.818 R_p=2.63 % wR_p=3.74 %	$Pm\bar{3}m$, a=b=c=4.0398(1) Å, α=β=γ=90 º					
	Ba	1a	0	0	0	0.0209(2)
	Fe	1b	0.5	0.5	0.5	0.0357(5)
	Ca	1b	0.5	0.5	0.5	0.0357(5)
	O	3c	0.5	0.5	0	0.0601(12)
x=0.10 χ^2=1.695 R_p=2.23 % wR_p=3.00 %	$Pm\bar{3}m$, a=b=c=4.0517(1) Å, α=β=γ=90 º					
	Ba	1a	0	0	0	0.0161(2)
	Fe	1b	0.5	0.5	0.5	0.0271(4)
	Ca	1b	0.5	0.5	0.5	0.0271(4)
	O	3c	0.5	0.5	0	0.0526(10)
x=0.15 χ^2=2.456 R_p=2.81 % wR_p=3.65 %	$Pm\bar{3}m$, a=b=c=4.0668(3) Å, α=β=γ=90 º					
	Ba	1a	0	0	0	0.0133(3)
	Fe	1b	0.5	0.5	0.5	0.0274(5)
	Ca	1b	0.5	0.5	0.5	0.0274(5)
	O	3c	0.5	0.5	0	0.0272(24)

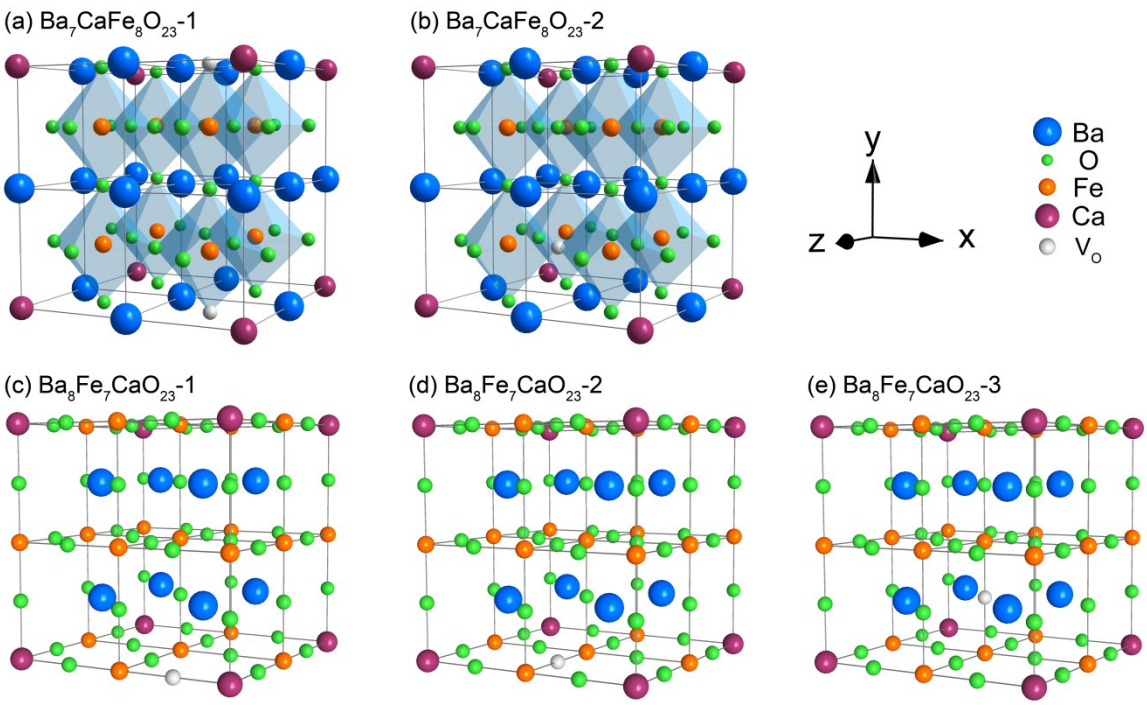

Fig. S2 The original defect models of Ca_{Ba} and Ca_{Fe} defects in $Ba_8Fe_8O_{23}$ supercells: (a) Ca_{Ba} neighboring to vacancy, (b) Ca_{Ba} away from vacancy, (c) Ca_{Fe} neighbouring to vacancy, (d) Ca_{Fe} second near to vacancy, (e) Ca_{Fe} away from vacancy.

Table S2 Tested molar ratio of three kinds of cations (Ba, Fe and Ca) in x=0.05 and 0.15 samples by EPMA.

x=0.05				x=0.15			
Point	Ba (%)	Fe (%)	Ca (%)	Point	Ba (%)	Fe (%)	Ca (%)
1	54.6	42.8	2.6	1	56.7	35.9	7.4
2	55.3	42.0	2.7	2	54.6	37.5	7.9
3	56.1	41.3	2.6	3	55.3	37.2	7.5
4	55.7	41.6	2.7	4	52.8	39.4	7.8
5	54.9	42.3	2.8	5	52.2	39.8	8.0
6	56.0	41.4	2.6	6	54.0	38.3	7.7
7	55.4	41.8	2.8	7	53.9	38.1	8.0
8	54.9	42.3	2.8	8	56.4	36.1	7.5
9	54.6	42.6	2.8	9	54.4	37.8	7.8
10	54.9	42.3	2.8	10	55.0	37.2	7.8
Average	55.8	41.6	2.6	Average	54.5	37.8	7.7

Table S3 Tested molar ratio of Ba, Fe and Ca cations in in x=0.05 and 0.15 samples by EDX.

x=0.05				x=0.15			
Point	Ba (%)	Fe (%)	Ca (%)	Point	Ba (%)	Fe (%)	Ca (%)
1	51.4	46.0	2.7	1	50.5	41.8	7.7
2	50.9	46.5	2.6	2	51.0	41.4	7.6

In order to confirm the chemical composition of B-site Ca-doped $BaFeO_{3-\delta}$ materials in a more accurate quantitative, EPMA technique was applied to analyse the molar ratio of the Ba, Fe and Ca cations for x=0.05 and x=0.15 samples as shown in Table S2. It was found that the combined molar fraction of Fe and Ca is similar to the that of Ba, and with increasing the Ca doping content to 0.15, the molar fraction of Ca increases to three times that of 0.05 sample, which follows well with the designed cation ratios of materials. The tested chemical composition by EDXS technique also shows similar results, as listed in Table S3. In addition, XRD refinements show that no impurity phases can be observed (Fig. S1) and surface elemental mapping reveals the uniform distribution of each element in the material (Fig. 2). These results strongly confirm that the Ca was successfully introduced to the B-site of $BaFeO_{3-\delta}$ materials. It should be mentioned that the error in EPMA results could come from the mixed oxidation states of Fe in Ca-doped $BaFeO_{3-\delta}$, as Fe_2O_3 was used as the reference material for Fe content determination in this measurement.

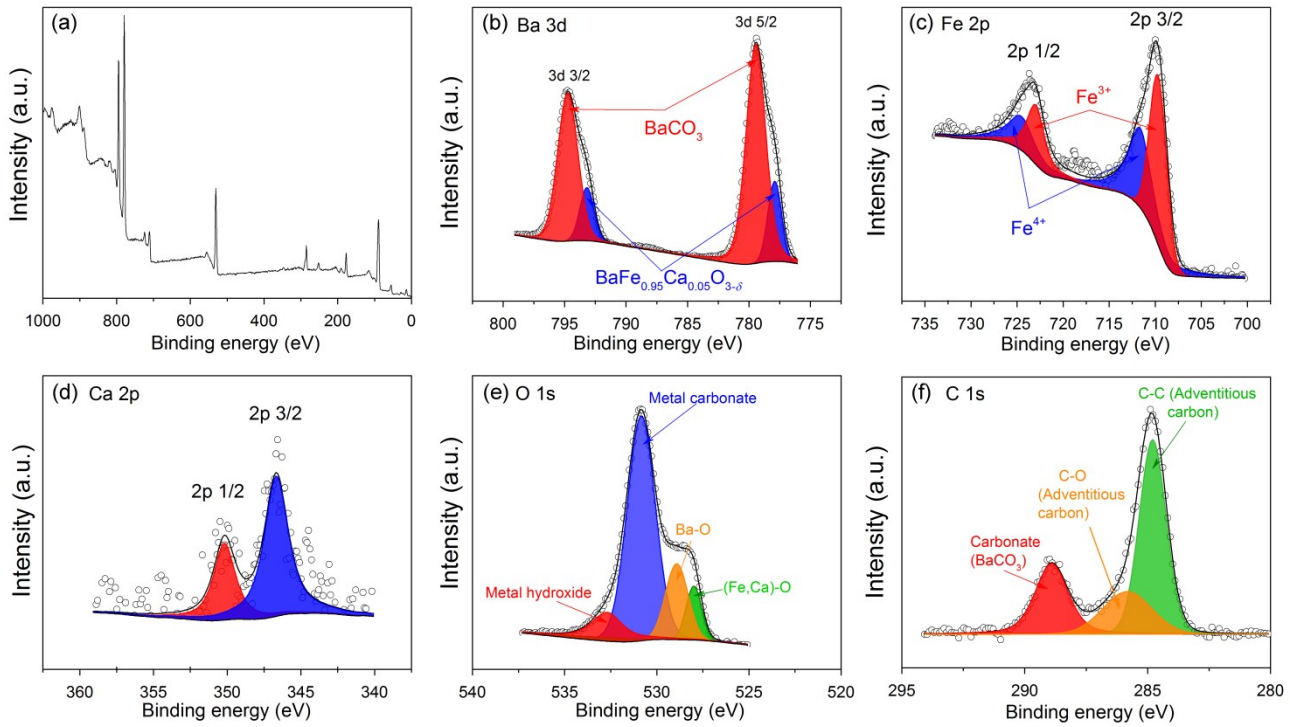

Fig. S3 XPS results of $BaFe_{0.95}Ca_{0.05}O_{3-\delta}$ sample (a), Ba 3d (b), Fe 2p (c), Ca 2p (d), O 1s (e) and C 1s(f).

In order to further confirm the occupation status of Ca cation in $BaFeO_{3-\delta}$, XPS measurements were carried out. Fig. S3 shows the core level XPS spectra of Ba 3d, Fe 2p, Ca 2p, O 1s and C 1s of $BaFe_{0.95}Ca_{0.05}O_{3-\delta}$ sample at room temperature. It can be seen that the spectra of Ca 2p can be fitted using single peak for both 2p3/2 and 2p1/2 levels, indicating the sole chemical environment of Ca in material, which should be 6-fold coordination according to the XRD, EPMA and EDXS results. [1-3] It should be mentioned that the formation of $CaCO_3$ cannot be excluded, but due to small amount of Ca, it cannot be unambiguously proven. Additionally, all Ca cannot be only present in the $CaCO_3$ phase, as such phase would be visible in other studies (XRD, EPMA, EDXS). Consequently, Ca has to be present in perovskite phase, and as Ca 2p signal (within limitation of the signal intensity) suggests single chemical environment, it is present at the B-site. Data analysis of the Fe 2p binding energy in $BaFe_{0.95}Ca_{0.05}O_{3-\delta}$ is depicted in Fig. S3 (c). Two chemical states could be identified in the Fe 2p spectrum corresponding to Fe3+ (709.8 eV and 723.0 eV, 58.4%) and Fe4+ (711.9 eV and 724.8 eV, 41.6%).[4] The calculated average of Fe valence (3.42) from the XPS results at room temperature is compatible with that based on oxygen deficiency (as discussed in the following Table S5). The asymmetric broad nature of Ba 3d spectra suggests that each of the spin-orbit peaks can be

deconvoluted into more than one peak, and two couples centered at 779.4 eV and 777.9 eV for Ba 3d5/2 and 793.2 eV and 794.8 eV for Ba 3d3/2 are fitted and compatible with Ba^{2+} element in barium carbonate and perovskite phase, respectively. Furthermore, the spectra of O 1s and C 1s envelope in Figs. S3e,f are characterized by binding energy peaks at 530.8 and 288.9 eV, which are corresponding to oxygen and carbon spectra for $BaCO_3$.[4-8] The propensity of Ba contained materials to form carbonates observed here were also highlighted in many published work.[9-11] Additionally, the low binding energy shoulder of C 1s peaks centered at (~285.8/284.8 eV) related to adventitious carbon species and the low binding energy shoulder of O 1s peaks (~528.0/528.9 eV) is ascribed to the Ba-O and (Fe,Ca)-O bonds in perovskite phase. It should be mentioned that there is an additional high binding energy peak of O 1s at 532.7 eV, which cna be possible attributed to the metal hydroxide.[4,8]

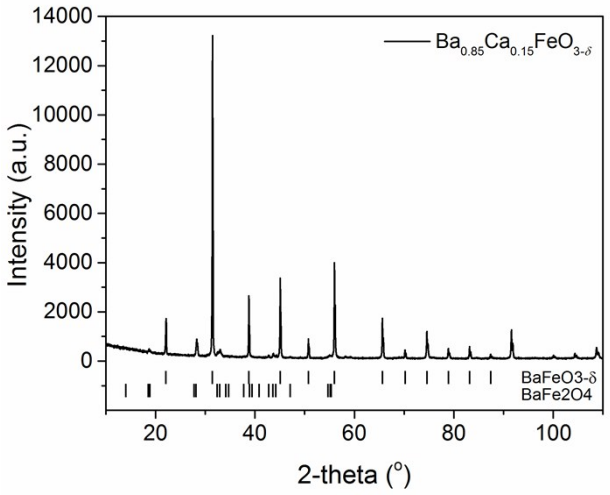

Fig. S4 Room temperature XRD result obtained for material with assumed $Ba_{0.85}Ca_{0.15}FeO_{3-\delta}$ composition.

As documented in Fig. S4, the material with Ca cations assumed to occupy A-site ($Ba_{0.85}Ca_{0.15}FeO_{3-\delta}$) was not a single phase, with cubic ($BaFeO_{3-\delta}$-like) and Fe-rich $BaFe_2O_4$-like phase present (on the other hand the assumed $BaFe_{0.85}Ca_{0.15}O_{3-\delta}$ composition was obtained as cubic, single phase). Presence of Ba:Fe with 1:2 ratio $BaFe_2O_4$ indicates that iron is expelled from the main phase, with only Ca cations being able to induce such the effect. In other words, because Ca cations cannot be (to a large extent) introduced at the A-site in $Ba_{0.85}Ca_{0.15}FeO_{3-\delta}$, but are located at the B-site. Consequently, in the main phase the Ba:Fe ratio (equal 0.85:1 by the assumption), becomes higher (closer to or even larger than one), which should yield a precipitate of another phase with much smaller Ba:Fe ratio - as what actually is in $BaFe_2O_4$. Obviously, it would be a speculation to say about

occupancy of Ca at different possible sites in such phases, but the observed results (together with initial results for $BaFe_{0.85}Ca_{0.15}O_{3-\delta}$) very strongly support the assumed Ca doping at the B-site.

Table S4 Rietveld parameters and refinement residuals obtained from HT-XRD patterns of samples with x=0.05 and 0.15 after cooling to 25 ˚C with assumption of the dopant to be present at A- or B-site.

Parameter	$BaFe_{0.95}Ca_{0.05}O_{3-\delta}$	$Ba_{0.95}Ca_{0.05}FeO_{3-\delta}$	$BaFe_{0.85}Ca_{0.15}O_{3-\delta}$	$Ba_{0.85}Ca_{0.15}FeO_{3-\delta}$
Ba (x, y, z)	(0, 0, 0)	(0, 0, 0)	(0, 0, 0)	(0, 0, 0)
Uiso (Å^2)	0.0209(2)	0.0198(2)	0.0133(3)	0.0114(4)
Occupation	1	0.95	1	0.85
Fe (x, y, z)	(0.5, 0.5, 0.5)	(0.5, 0.5, 0.5)	(0.5, 0.5, 0.5)	(0.5, 0.5, 0.5)
Uiso (Å^2)	0.0357(5)	0.0198(2)	0.0274(5)	0.0114(4)
Occupation	0.95	1	0.85	1
Ca (x, y, z)	(0.5, 0.5, 0.5)	(0, 0, 0)	(0.5, 0.5, 0.5)	(0, 0, 0)
Uiso (Å^2)	0.0357(5)	0.0410(5)	0.0274(5)	0.0459(6)
Occupation	0.05	0.05	0.15	0.15
χ^2	2.818	2.914	2.456	2.878
R_p (%)	2.63	2.66	2.81	2.94
wR_p (%)	3.74	3.80	3.65	3.95

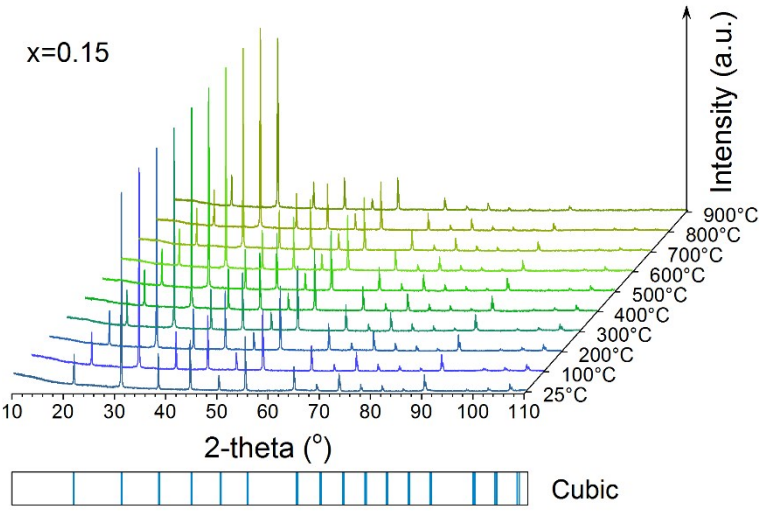

Fig. S5 *In situ* XRD patterns of x = 0.15 sample from 25 to 900 °C under air atmosphere.

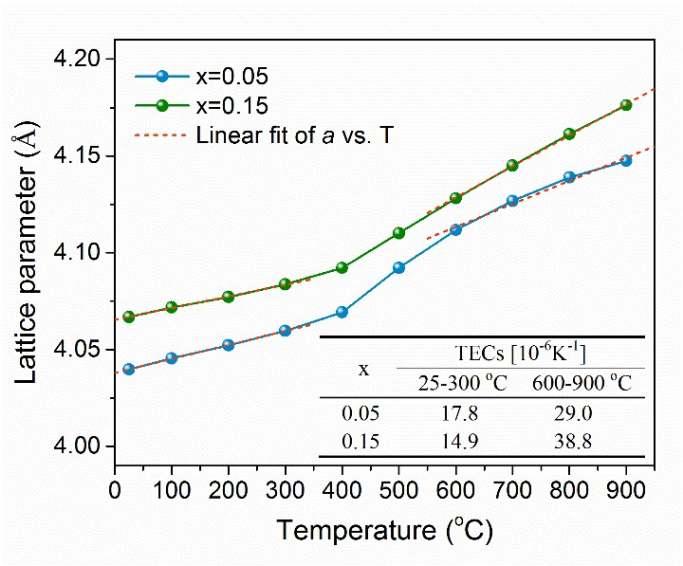

Fig. S6 Temperature dependence of lattice parameter for $BaFe_{1-x}Ca_xO_{3-\delta}$ samples with x = 0.05 and 015. Inset: fitted TECs results.

For sample x=0.025, there is a sudden weight loss in the middle temperature range of cooling curves, which reversibly occurs in the following thermal cycles. The start temperature of the abnormal weight loss in first cooling process corresponds well to the phase transition temperature from cubic to triclinic structure (Fig. 3a) and the fully stabilized samples x=0.05 and 0.15 with cubic structure do not show this phenomenon.

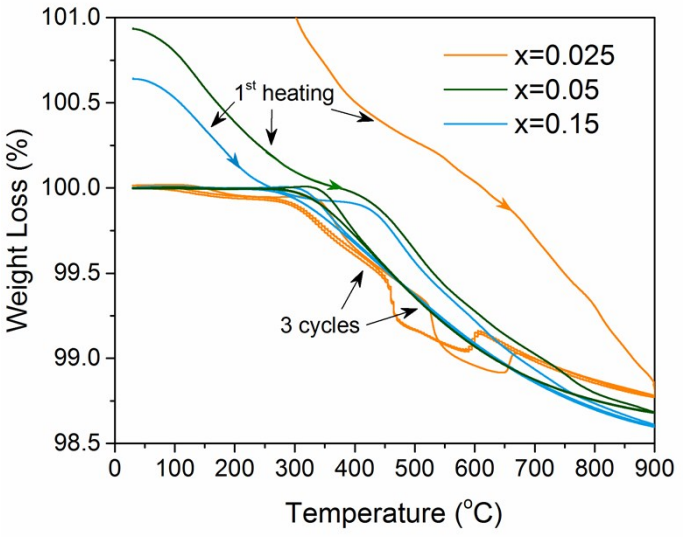

Fig. S7 TG curves of $BaFe_{1-x}Ca_xO_{3-\delta}$ (x=0.025, 0.05 and 0.15) for respective 3 thermal cycles in air.

Table S5 Calculated oxygen nonstoichiometry (δ) and average valence of Fe ($\bar{N}$) at different temperatures of samples $BaFe_{1-x}Ca_xO_{3-\delta}$ (x = 0.025, 0.05 and 0.015).

x	Oxygen deficiency (δ)			Average valence of Fe		
	900 °C	800 °C	25 °C	900 °C	800 °C	25 °C
0.025	0.56	0.55	0.38	2.90	2.92	3.27
0.05	0.55	0.54	0.35	2.96	2.98	3.36
0.15	0.52	0.51	0.32	3.12	3.16	3.60

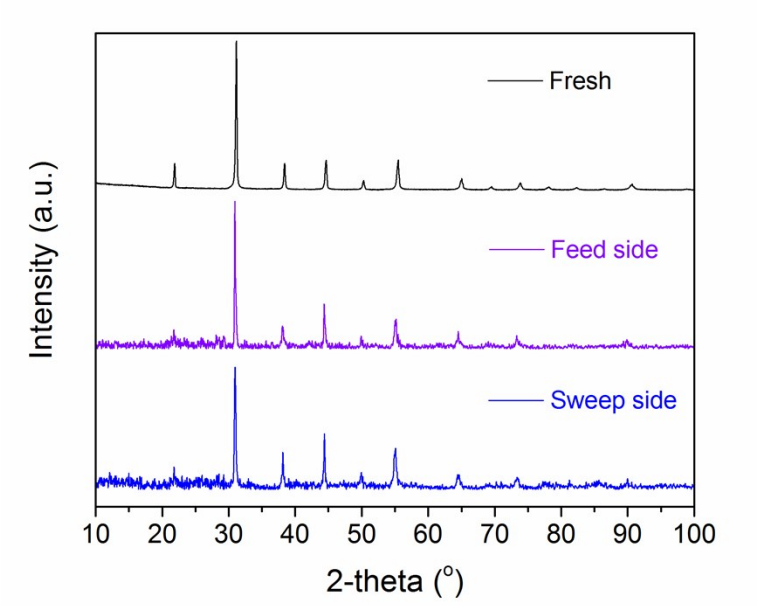

Fig. S8 XRD patterns of both sides of $BaFe_{0.95}Ca_{0.05}O_{3-\delta}$ membrane after long term permeation measurement.

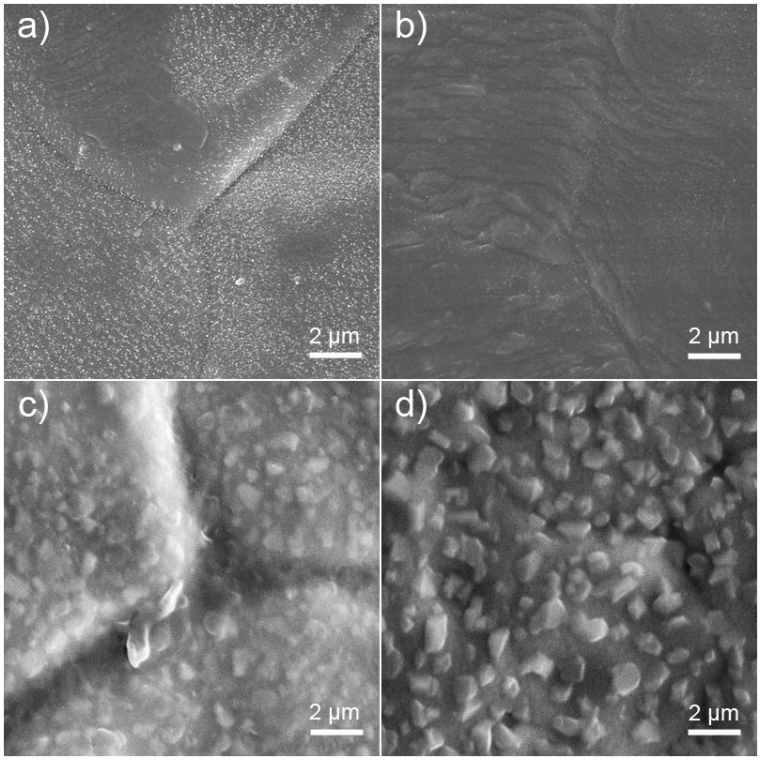

Fig. S9 Surface morphologies of $BaFe_{1-x}Ca_xO_{3-\delta}$ membranes with x= 0.05 and 0.15 treated in 5 vol% H_2/Ar (a, b) and 2 vol% CO_2/N_2 (c, d) at 800 °C for 8 h, respectively.

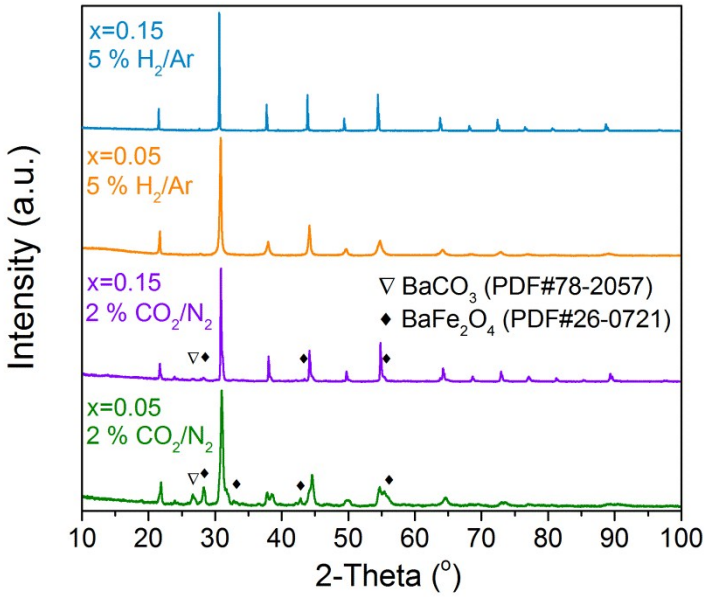

Fig. S10 Surface XRD patterns of $BaFe_{1-x}Ca_xO_{3-\delta}$ membranes with x= 0.05 and 0.15 treated in 5 vol% H_2/Ar and 2 vol% CO_2/N_2 at 800 °C for 8 h, respectively.

References

[1] S. Wang, Y. Chen, S. Fang, L. Zhang, M. Tang, K. An, K. S. Brinkman and F. Chen, *Chem. Mater.*, 2014, **26**, 2021.

[2] A. Dutta, S. Saha, P. Kumari, T. P. Sinha and S. Shannigrahi, *J. Solid State Chem.*, 2015, **229**, 296.

[3] R. Dudric, A. Vladescu, V. Rednic, M. Neumann, I. G. Deac and R. Tetean, *J. Mol. Struct.*, 2014, **1073**, 66.

[4] J. Stoch and J. Gablankowska-Kukucz, *Surf. Interface Anal.*, 1991, **17**, 165.

[5] M. Brisotto, F. Cernuschi, F. Drago, C. Lenardi, P. Rosa, C. Meneghini, M. Merlini and C. Rinaldi, *J. Eur. Ceram. Soc.*, 2016, **36**, 1679.

[6] P. J. Schmitz, *Surf. Sci. Spectra*, 2001, **8**, 190.

[7] M. Wegmann, *J. Am. Ceram. Soc.*, 2004, **87**, 371.

[8] H. Falcón, J. A. Barbero, J. A. Alonso, M. J. Martínez-Lope and J. L. G. Fierro, *Chem. Mater.*, 2002, **14**, 2325.

[9] J. Jung and D. D. Edwards, *J. Solid State Chem.*, 2011, **184**, 2238

[10] M. Arnold, H. Wang and A. Feldhoff, *J. Membr. Sci.*, 2007, **293**, 44.

[11] Z. Shao, G. Xiong, H. Dong, W. Yang and L. Lin, *Sep. Purif. Technol.*, 2001, **25**, 97.